NASA MEMO 2-3-59L

NASA MEMO 2-3-59L

NASA

MEMORANDUM

COMPARISON OF CONTROL-FIXED STABILITY DERIVATIVES FOR TWO SUPERSONIC FIGHTER AIRPLANES AS DETERMINED FROM FLIGHT AND WIND-TUNNEL TESTS

By Harold L. Crane, Milton D. McLaughlin, and Jack A. White

Langley Research Center
Langley Field, Va.

NATIONAL AERONAUTICS AND SPACE ADMINISTRATION
WASHINGTON
April 1959

[redacted]

NATIONAL AERONAUTICS AND SPACE ADMINISTRATION

MEMORANDUM 2-3-59L

COMPARISON OF CONTROL-FIXED STABILITY DERIVATIVES FOR TWO SUPERSONIC FIGHTER AIRPLANES AS DETERMINED FROM FLIGHT AND WIND-TUNNEL TESTS*

By Harold L. Crane, Milton D. McLaughlin, and Jack A. White

SUMMARY

The principal control-fixed stability derivatives of two fighter airplanes operating in the clean condition have been obtained from flight tests at an altitude of 35,000 feet at Mach numbers up to 1.44 for one airplane and up to 1.23 for the other airplane. The static derivatives were compared with those determined from wind-tunnel results after the tunnel data were adjusted for the effects of differences in configuration, aeroelastic distortion, and mass flow through the engine. After these adjustments were made, the static derivatives determined from the wind-tunnel results usually proved to be an adequate indication of the derivatives of the full-scale airplane.

INTRODUCTION

The principal control-fixed stability derivatives of two modern fighter airplanes have been determined from the characteristics of the short-period longitudinal and lateral oscillations measured in flight. The purpose of this paper is to present the stability derivatives obtained from the flight tests of these two airplanes and, insofar as possible, to compare the stability derivatives determined from flight with those previously determined from wind-tunnel measurements of the two airplane configurations. The results are presented for a Mach number range of approximately 0.7 to 1.44 for airplane A and 0.7 to 1.23 for airplane B. The flight data were obtained at an altitude of approximately 35,000 feet to minimize the required correction of wind-tunnel results for the aeroelastic distortion of the airframe.

*Title, Unclassified.

[redacted]

The longitudinal derivatives were determined by use of the approximate mathematical expressions which may be found in various papers. (See ref. 1, for example.) The lateral derivatives have been determined from the flight records by the time-vector method which has been described in previous papers. (See refs. 2 to 4.) The static derivatives which were available from NASA wind-tunnel results (refs. 5 and 6) obtained in the Langley 8-foot transonic tunnels and the Langley 4- by 4-foot supersonic pressure tunnel are compared to the values obtained from the flight data. The wind-tunnel results have been adjusted, whenever the correction was appreciable, in accordance with the estimated flexibility and/or engine mass-flow characteristics of each airplane which were supplied by the manufacturers.

Additional results of the flight measurements of handling qualities of airplane A are presented in reference 7.

SYMBOLS AND COEFFICIENTS

The results of this investigation are referred to the stability system of axes, which is defined as a three-dimensional right-hand orthogonal system of axes intersecting at the airplane center of gravity in which the X- and Z-axes lie in the plane of symmetry. The X-axis is the projection of the relative airstream onto the XZ-plane of symmetry. The Y- and Z-axes are perpendicular to the X-axis and to each other.

a_y lateral acceleration, g units

a_z normal acceleration, g units

b wing span, ft

c wing chord, ft

$\bar{c}$ mean aerodynamic chord of wing, ft

$\bar{c}_t$ mean aerodynamic chord of tail, ft

C_L lift coefficient, W/qS

C_{L_α} lift-curve slope, $\frac{\partial C_L}{\partial \alpha}$, per radian

C_l rolling-moment coefficient, $\frac{\text{Rolling moment}}{qSb}$

C_{l_p} damping-in-roll derivative, $\frac{\partial C_l}{\partial\left(\frac{pb}{2V}\right)}$, per radian

C_{l_r} rate of change of rolling-moment coefficient with yawing angular-velocity factor, $\frac{\partial C_l}{\partial\left(\frac{rb}{2V}\right)}$, per radian

C_{l_β} effective-dihedral derivative, $\frac{\partial C_l}{\partial \beta}$

C_m pitching-moment coefficient, $\frac{\text{Pitching moment}}{qS\bar{c}}$

$C_{m_{C_L}}$ static margin, mean chord units

C_{m_q} $\frac{\partial C_m}{\partial\left(\frac{q\bar{c}}{2V}\right)}$, per radian

C_{m_α} longitudinal-stability derivative, $\frac{\partial C_m}{\partial \alpha}$, per radian

$C_{m_{\dot{\alpha}}}$ $\frac{\partial C_m}{\partial\left(\frac{\dot{\alpha}\bar{c}}{2V}\right)}$, per radian

C_n yawing-moment coefficient, $\frac{\text{Yawing moment}}{qSb}$

C_{n_p} rate of change of yawing-moment coefficient with rolling angular-velocity factor, $\frac{\partial C_n}{\partial\left(\frac{pb}{2V}\right)}$, per radian

C_{n_r} rate of change of yawing-moment coefficient with yawing angular-velocity factor, $\frac{\partial C_n}{\partial\left(\frac{rb}{2V}\right)}$, per radian

C_{n_β} directional-stability derivative, $\frac{\partial C_n}{\partial \beta}$, per radian

$C_{n_{\dot{\beta}}}$ rate of change of yawing-moment coefficient with rate of change of angle-of-sideslip factor, $\frac{\partial C_n}{\partial\left(\frac{\dot{\beta} b}{2V}\right)}$, per radian

C_Y lateral-force coefficient, $\frac{\text{Lateral force}}{qS}$

C_{Y_p} rate of change of lateral-force coefficient with rolling angular-velocity factor, $\frac{\partial C_Y}{\partial\left(\frac{pb}{2V}\right)}$, per radian

C_{Y_r} rate of change of lateral-force coefficient with yawing angular-velocity factor, $\frac{\partial C_Y}{\partial\left(\frac{rb}{2V}\right)}$, per radian

C_{Y_β} rate of change of lateral-force coefficient with angle of sideslip, $\frac{\partial C_Y}{\partial \beta}$, per radian

$C_{Y_{\dot{\beta}}}$ rate of change of lateral-force coefficient with rate of change of angle-of-sideslip factor, $\frac{\partial C_Y}{\partial\left(\frac{\dot{\beta} b}{2V}\right)}$, per radian

D differential operator, $\frac{d}{d\,\frac{Vt}{c}}$

g acceleration due to gravity, ft/sec^2

I_Y moment of inertia about Y stability axis

K_X nondimensional radius of gyration in roll about X stability axis

K_Z nondimensional radius of gyration in yaw about Z stability axis

K_{XZ} nondimensional product-of-inertia parameter

M Mach number

m mass of airplane, W/g, slugs

P period of damped natural frequency, sec

p rolling velocity, radians/sec

$\dot{p} = \frac{dp}{dt}$, radians/sec^2

q dynamic pressure, $\frac{1}{2}\rho V^2$, lb/sq ft; pitching velocity, radian/sec

$\dot{q} = \frac{dq}{dt}$, radians/sec^2

r yawing velocity, radians/sec

$\dot{r} = \frac{dr}{dt}$, radians/sec^2

S wing area, sq ft

$T_{1/2}$ time required for transient oscillation to damp to one-half amplitude, sec

t time, sec

V airspeed, ft/sec

W weight of airplane, lb

Y side force or lateral force, lb

Y_β aerodynamic component of side force due to angle of sideslip

$Y_{\dot{\beta}}$ aerodynamic component of side force due to lag in sidewash

Y_ϕ weight component of side force due to angle of bank

$Y_{\dot{\psi}}$ inertial component of side force due to yawing velocity

α angle of attack of airplane, angle between reference body X-axis and stability X-axis, deg

$\dot{\alpha} = \frac{d\alpha}{dt}$, radians/sec

β angle of sideslip, deg or radians

$\dot{\beta} = \frac{d\beta}{dt}$, radians/sec

ρ mass density of air, slugs/cu ft

ϕ angle of bank (positive with right wing down), radian

ψ angle of yaw (positive with nose right), radian

$\dot{\psi} = \frac{d\psi}{dt}$, radians/sec

μ relative-density factor, $m/\rho Sb$

DESCRIPTION OF THE AIRPLANES

Airplane A is a high-wing, low-tail fighter airplane with the wing having 42° of sweepback of the quarter-chord line. Photographs of the test airplane are shown in figure 1, a three-view drawing of the airplane is given in figure 2, and pertinent dimensions of the physical characteristics of the airplane are presented in table I. The airplane normally employs equipment to provide automatic stabilization about the roll and yaw axes and also to provide interconnection of rudder and aileron controls during manual operation, but this equipment was turned off during the present tests. The tests were conducted in the cruise configuration (flaps and gear up). At subsonic and transonic velocities, the so-called cruise droop was employed, as is customary, to improve the cruise and maneuver performance. Cruise droop consists of deflection of the leading-edge flap on the wing which produces an effective camber in the wing. The deflection of the leading-edge flap is 6.8° and 7.0° for the inboard and outboard sections, respectively. (See fig. 2.)

Airplane B is a midwing fighter airplane with the wing having 35° of sweepback of the quarter-chord line. The horizontal tail is mounted slightly lower than the wing. A three-view drawing of the airplane is shown in figure 3, the pertinent dimensions of the physical characteristics of the airplane are presented in table II, and photographs of airplane B are shown in figure 4. For flight with flaps retracted,

longitudinal control was provided by an all-movable horizontal tail. With the flaps extended, additional pitch control was provided by a geared elevator. Lateral control was provided by flaperons (spoilers) mounted ahead of the flaps. The rudder control was conventional. Although the airplane was equipped with a yaw damper which operated the rudder, the yaw damper was turned off and the data presented herein were for the airplane in the clean condition and with power for level flight.

TEST CONDITIONS

Wind Tunnel

The wind-tunnel data which were used herein for comparison with flight-test results were obtained from references 5 and 6. The data for Mach numbers up to 1.2 were obtained in the Langley 8-foot transonic tunnels whereas the data for a Mach number of 1.4 were obtained in the Langley 4- by 4-foot supersonic pressure tunnel. The scale of the model of airplane A (ref. 5) was 0.042 and of airplane B (ref. 6) was 0.067. The test Reynolds number was approximately 2,000,000 over the test Mach number range for both configurations.

The models were mounted on a sting. The tare force along the longitudinal body axis was adjusted so that the magnitude corresponded to that which would be produced by a pressure at the model base equal to the free-stream static pressure. Sting interference and buoyancy corrections were considered to be negligible. At subsonic speeds, the wall interference effects were also considered to be within the accuracy of the data. For Mach numbers between 1.03 and 1.12, the effects of wall-reflected disturbances were considered to be large, and no measured data were used in this speed range. At other supersonic speeds, the effects of wall-reflected disturbances were considered to be small and were neglected.

In neither case was the model configuration exactly the same as the test airplane configuration. The principal differences between the model configuration and airplane A were in the longitudinal fuselage dimensions. These changes consisted mainly of a fuselage extension on the airplane of approximately 2 feet (at full scale) behind the horizontal tail. Since the tail length was not changed by this modification, no adjustment of the tunnel data for configuration discrepancies has been made in the present paper for the model of airplane A. The wind-tunnel data presented herein for the model of airplane B have been adjusted for differences in tail length and area of the vertical tail between the wind-tunnel model and the airplane by adjusting the increment between tail-on and tail-off wind-tunnel data for the changes in configuration. The area of the vertical tail of the airplane was 23 percent greater than that which was represented by the model. The tail length was 6 percent greater.

These were the only known significant differences between airplane B and the wind-tunnel model.

Flight

The flight tests were made by initiating small longitudinal or lateral disturbances from trimmed level flight at an altitude of approximately 35,000 feet. Examples of the short-period oscillations which resulted are shown in figures 5 and 6. The test center-of-gravity ranges were 27.5 to 28 percent $\bar{c}$ for airplane A and 24 to 25 percent $\bar{c}$ for airplane B. A table of approximate trim lift coefficients follows:

M	C_L for -	
	Airplane A	Airplane B
0.7	----	0.36
.8	0.30	.32
.9	.23	.25
1.0	.16	.21
1.1	.12	.18
1.2	.10	.15
1.3	.09	----
1.4	.07	----

FLIGHT INSTRUMENTS AND ACCURACY

Standard NASA instruments were used in both airplanes to record airspeed, altitude, three components of angular velocity and acceleration, lateral and normal components of linear acceleration, angles of attack and sideslip, and control positions. The pitot-static head and the sideslip and angle-of-attack vanes were all mounted on a nose boom as shown in figures 1, 2, and 4. All records in either airplane were synchronized at 0.1-second intervals by a common timing circuit.

The turnmeters used to measure angular velocities and accelerations were referenced to the body axes of the airplane. Alinement errors were less than 0.5° for the turnmeters and linear accelerometers. Because the accelerometers were necessarily mounted away from the center of gravity, the linear-acceleration data were corrected for the effects of angular acceleration. The turnmeters and accelerometers are considered to be accurate to within approximately ±1.0 percent of the scale ranges.

The indicated angles of sideslip and angles of attack, measured by vane-type sensors, were corrected by the vector methods of reference 2 for yawing-velocity and pitching-velocity effects, respectively. The corrections to the vane readings for rolling velocity were considered to be negligible. The vanes were mass balanced and had essentially flat frequency response characteristics over the frequency range of airplane motions. The vane indications were statically accurate to about ±0.1°.

The differences in instrument lag were considered when the phasing and amplitude of the various measured quantities were determined from the flight records.

The scale ranges, sensitivities, and dynamic characteristics of the instruments used to measure the dynamic response of airplanes A and B are presented in the following table:

Measured quantities	Approximate scale range	Sensitivity per inch of film		Natural frequency, undamped, cps		Damping ratio	
	Airplanes A and B	Airplane A	Airplane B	Airplane A	Airplane B	Airplane A	Airplane B
α, deg	-10 to +30	11.3	10.5	10 to 20	10 to 20	[c]0.1	[c]0.1
β, deg	±40	10.6	9.7	10 to 20	10 to 20	[c]0.1	[c]0.1
p, radians/sec	±4	3.8	3.9	18.5	18.5	0.57	0.65
$\dot{p}$, radians/sec^2	±6 or [a]±10	6.0	10.0	7	7.1	0.68	0.65
q, radians/sec	±0.5	0.50	0.48	18.5	9.5	0.59	0.60
$\dot{q}$, radians/sec^2	±0.8	0.76	0.78	7	7	0.65	0.68
r, radians/sec	±0.5	0.49	0.48	9.5	14.25	0.60	0.61
$\dot{r}$, radians/sec^2	±0.8	0.79	0.79	7	7.0	0.68	0.65
a_z, g units	[b] 0 to 2	0.99	1.0	14	12	0.67	0.7
	[b] -1 to 6	3.5	3.6	24	25.5	0.69	0.7
a_y, g units	±0.5	1.0	1.0	13.5	13.5	0.66	0.7

[a] Airplane B.
[b] Accelerometers of two sensitivities were used.
[c] Conditions at sea level.

METHOD

Longitudinal Stability Derivatives

The longitudinal derivatives C_{m_α} and $C_{m_q} + C_{m_{\dot{\alpha}}}$ were determined by substituting the measured values of period and damping of the short-period longitudinal oscillation in the following expressions:

$$C_{m_\alpha} = -\frac{I_Y}{\frac{1}{2}\rho V^2 S\bar{c}}\left[\left(\frac{2\pi}{P}\right)^2 + \left(\frac{0.693}{T_{1/2}}\right)^2\right]$$

$$C_{m_q} + C_{m_{\dot{\alpha}}} = \frac{4I_Y V}{\frac{1}{2}\rho V^2 S\bar{c}^2}\left(\frac{C_{L_\alpha}\rho VS}{4m} - \frac{0.693}{T_{1/2}}\right)$$

These expressions have previously appeared in other reports. (See ref. 1, for example.) The lift-curve slope, which is needed in the solution of the damping derivative, was determined from the flight measurements of the amplitude ratio of normal acceleration to angle of attack during the short-period oscillation. The moment of inertia was determined as a function of airplane loading from calculated data furnished by the manufacturers. A first approximation of the derivative $\partial C_m/\partial C_L$ was determined by taking the ratio of C_{m_α} to C_{L_α}.

Lateral Stability Derivatives

The time-vector method was used for determining the lateral stability derivatives from flight measurements. The lateral equations of motion in vector form, based on those of reference 4 but including rate of change of sideslip terms, are as follows:

$$-C_{Y_\beta} - \frac{1}{2}C_{Y_p}\frac{D\phi}{\beta} - \frac{1}{2}C_{Y_r}\frac{D\psi}{\beta} - \frac{1}{2}C_{Y_{\dot{\beta}}}\frac{D\beta}{\beta} + 2\mu D\left(1 + \frac{\psi}{\beta}\right) - C_L\frac{\phi}{\beta} = 0 \qquad (1)$$

$$-C_{l_\beta} - \frac{1}{2}C_{l_p}\frac{D\phi}{\beta} - \frac{1}{2}C_{l_r}\frac{D\psi}{\beta} - \frac{1}{2}C_{l_{\dot{\beta}}}\frac{D\beta}{\beta} + 2\mu D\left(\frac{D\phi}{\beta}K_X{}^2 - \frac{D\psi}{\beta}K_{XZ}\right) = 0 \qquad (2)$$

$$-C_{n_\beta} - \frac{1}{2} C_{n_p} \frac{D\phi}{\beta} - \frac{1}{2} C_{n_r} \frac{D\psi}{\beta} - \frac{1}{2} C_{n_{\dot{\beta}}} \frac{D\beta}{\beta} + 2\mu D\left(\frac{D\psi}{\beta} K_Z^2 - \frac{D\phi}{\beta} K_{XZ}\right) = 0 \quad (3)$$

In the three lateral equations of motion, three degrees of freedom, each with the same frequency and damping characteristics, are involved in each equation: namely, sideslip, roll, and yaw. The motions represented by these three equations have the same damping rate, and the phase angles remain constant; thus, for vector representation, the various amplitude and phase relations are invariant with time. The $C_{Y_{\dot{\beta}}}$ and $C_{l_{\dot{\beta}}}$ terms are not considered directly in the present evaluation. In the application of the yawing-moment equation (eq. (3)), $D\beta$ is assumed to be equal and opposite to $D\psi$. This assumption has a negligible effect on the accuracy of the solution of this equation and permits evaluation of the combined derivative $C_{n_r} - C_{n_{\dot{\beta}}}$.

The lateral stability derivatives and the equations of motion employed in the present analysis are referenced to the stability system of axes. Inasmuch as the flight data are referenced to the body axes, the flight data were transferred from the body axes to the stability axes by the method described in reference 2.

The vector method of references 2 and 3 was employed for the determination of C_{n_β}, $C_{n_r} - C_{n_{\dot{\beta}}}$, C_{l_β}, and C_{l_p}. Experience has shown that the values of C_{Y_p} and C_{Y_r} may often be neglected in calculating the lateral motion. In order to examine the possible effects of assuming C_{Y_p} and C_{Y_r} to be equal to zero, the C_{Y_p} and C_{Y_r} vectors for three representative flight records were determined from the manufacturer's design values of these derivatives. These vectors proved to be very small, and their sum was negligible. It was therefore assumed throughout the present analysis that C_{Y_p} and C_{Y_r} were equal to zero. It was also necessary to assume values for one derivative in order to solve each moment equation. Estimated values of C_{n_p} and C_{l_r} furnished by the manufacturers were used inasmuch as these quantities determine vectors of minor importance to the equilibrium of moments.

Since C_{Y_p} and C_{Y_r} were found to be negligible, it was possible to determine C_{Y_β} by means of the following simplified equation derived from equation (1):

$$C_{Y_\beta} = 2\mu D + 2\mu \frac{D\psi}{\beta} - C_L \frac{\phi}{\beta} \qquad (4)$$

or directly from the measured lateral acceleration as follows:

$$C_{Y_\beta} = \frac{a_y W}{\beta q S} \qquad (4a)$$

In addition, since all three terms of equation (4) were available from measurements, these data were checked for consistency with the lateral-accelerometer data. A graphical illustration of a vector solution of equations (4) and (4a) for one test record is shown in figure 7. It will be noted that the vector diagram did not close until adjustments were made to the measured data.

Both a correction in phase angle and a change in amplitude of one of the vectors representing the inertia terms were required to close the vector diagram of figure 7. It was assumed that the discrepancy was much more likely to be due to some sidewash effect at the vane than to an error in the measurement of angular velocity. Therefore, the $\dot{\beta}$ and β vectors were adjusted as needed to satisfy the equation while $\dot{\beta}/\beta$ was held constant. The amplitudes of β and $\dot{\beta}$ were thereby reduced about 10 percent for airplane A and as much as 25 percent for airplane B to satisfy the side-force equation with the result that the values determined for C_{Y_β}, C_{l_β}, and C_{n_β} were increased in the same ratio. The required adjustments of the phase angle of the β vectors were typically 5° and sometimes as much as 10°. Phase discrepancies of this magnitude primarily affect the determination of $C_{n_r} - C_{n_{\dot{\beta}}}$ and C_{l_p} and could cause errors of 50 percent or more in these derivatives.

RESULTS

General Discussion

The control-fixed stability derivatives obtained from measurements made in flight are presented in figures 8 to 13. The static derivatives are compared with values obtained from wind-tunnel measurements. The fact that the flight results are for 1 g operation at a pressure altitude of approximately 35,000 feet tends to minimize the effects of aeroelastic distortion which must be considered when comparing stability derivatives from flight and tunnel tests. However, in instances in which the distortion effects based on estimates by the manufacturers, became as large as 5 percent of the value of a derivative, the wind-tunnel results have been adjusted accordingly. The estimates of flexibility effects assumed

the fuselage to be rigid but the wing and tail surfaces to be flexible. Adjustments were made for changes in lift-curve slope of the tail surface as well as for changes in the lift-curve slope and the aerodynamic-center position of the wing.

The wind-tunnel tests for airplane A did not simulate the engine mass-flow effects. Therefore, the appropriate derivatives obtained from the wind-tunnel tests have been adjusted for mass-flow effects by the method used in reference 2. During the tunnel tests of the model of airplane B, mass-flow through the fuselage ducts approximated the flight values well enough to make further adjustments for mass-flow effects unnecessary.

Longitudinal Stability Derivatives

The longitudinal stability derivatives C_{L_α}, C_{m_α}, $C_{m_{C_L}}$, and $C_{m_q} + C_{m_{\dot{\alpha}}}$ which were determined from flight measurements are presented in figures 8 and 9 for airplanes A and B, respectively. Wind-tunnel values for the static derivatives obtained from references 5 and 6 are also shown. For airplane A, the wind-tunnel and flight values of C_{L_α} are in reasonable agreement. However, a comparison of the pitching-moment derivatives reveals poorer agreement. The wind-tunnel results indicate a somewhat lower degree of longitudinal stability than do the flight results (a decrement of 5 percent in the static margin) and a later transonic stability change which occurred at a Mach number of approximately 0.90 as compared to the flight value of 0.85. The cruise droop was used for the subsonic flight tests but not for the wind-tunnel results shown in figure 8. However, wind-tunnel tests including the cruise droop were available for a more limited range of Mach numbers, and these data showed that the cruise droop caused a rearward aerodynamic-center shift of about $0.01\bar{c}$ compared with the discrepancy of $0.05\bar{c}$ between flight and tunnel results. Thus far, no explanation has been found for the difference between wind-tunnel and flight values of critical Mach number. The total transonic aerodynamic-center shift was indicated to be about 15 percent $\bar{c}$ in either case.

For airplane B, the lift-curve slope measured in flight was approximately 5 percent lower than the wind-tunnel value. The flight and wind-tunnel values for pitching-moment derivatives shown in figure 9 had approximately parallel trends with Mach number although the wind-tunnel results indicated a 5 to 10 percent smaller static margin. The transonic aerodynamic-center shift was about 35 percent of the mean aerodynamic chord for airplane B.

Reference 8 presents longitudinal-stability data for airplane B obtained in the 8-foot wind tunnel of the Cornell Aeronautical Laboratory. The variation of static margin with Mach number as determined from the data of reference 8 was indicated to fall between the values shown for flight and wind-tunnel results obtained at Langley Research Center over most of the test Mach number range.

As would be expected, the slope of the lift curve of airplane A which a 42° sweptback wing was somewhat lower than that of airplane B which had a 35° sweptback wing. The transonic aerodynamic-center shift was at least twice as great for airplane B as for airplane A, but the fact that the maximum rate of change of aerodynamic-center position with Mach number was about the same for either airplane was apparently more significant to the pilot. The level of the pitch damping for airplane B was also greater than for airplane A and approximately doubled in the transonic range, while the damping for airplane A decreased gradually with increasing Mach number. Closer examination of the results for airplane B (fig. 9) indicated that the improved transonic and supersonic pitch damping of airplane B only occurred when the pilot released the stick or relaxed slightly his grip on the stick and thus permitted the bobweights to move the control as a function of the normal and angular acceleration. The phasing was such that the damping in pitch was thereby improved. The resulting motion of the stick was usually not noticed by the pilot. The stick force required to oppose the bobweights was only 4 or 5 pounds. (See fig. 5.)

Lateral Stability Derivatives

The lateral stability derivatives C_{n_β}, C_{l_β}, C_{Y_β}, C_{l_p}, and $C_{n_r} - C_{n_{\dot{\beta}}}$, which were determined from flight measurements, are presented in figures 10 to 13 for airplanes A and B. The values assigned to C_{n_p} and C_{l_r} for use in this evaluation are also shown in figures 12 and 13 and are based on the estimates of the manufacturers. Values determined in transonic and supersonic wind tunnels for C_{n_β}, C_{l_β}, and C_{Y_β} are also shown for comparison with the flight results. These wind-tunnel derivatives have been corrected for estimated aeroelastic distortion and mass-flow effects whenever the estimated corrections were appreciable. Note that the wind-tunnel values of C_{n_β} and C_{l_β} are at nearly the same level as the derivatives measured in flight. However, the short-range trends with Mach number indicated by the flight and wind-tunnel results were sometimes quite different (as

in the case of C_{l_β} or C_{n_β} for airplane B). The moderate amount of scatter which is present in the flight results could conceal some of the short-range trends indicated by the wind-tunnel tests. The flight values of C_{Y_β} were usually about 20 percent smaller than the wind-tunnel values.

It is interesting to note that all the measured lateral derivatives except the damping-in-yaw derivative $C_{n_r} - C_{n_{\dot\beta}}$ were approximately of equal magnitude for airplanes A and B and were not subject to large variation with Mach number. The values of $C_{n_r} - C_{n_{\dot\beta}}$ determined in flight for airplane A decreased gradually from approximately -0.6 to approximately -0.4 with increasing Mach number. The values for airplane B were more erratic and the yaw damping was much less with the level of $C_{n_r} - C_{n_{\dot\beta}}$ approximating -0.1. It should be emphasized that the lateral stability derivatives were measured with the yaw-damping devices turned off. The assigned values of C_{n_p} and C_{l_r}, which were based on estimates of the manufacturers, were at approximately the same level for airplanes A and B at the minimum test Mach number but had dissimilar trends with increasing Mach number.

CONCLUDING REMARKS

Stability derivatives determined from data obtained at the Langley 8-foot transonic tunnels and the Langley 4- by 4-foot supersonic pressure tunnel for models of airplanes A and B, when corrected for mass-flow effects and aeroelastic distortion, usually agreed with the stability derivatives of the full-scale airplanes within acceptable limits. However, the directional-stability derivative C_{n_β} and the effective-dihedral derivative C_{l_β} for airplane B were indicated by the wind-tunnel results to have more erratic variation with Mach number than was measured in flight. Another discrepancy between flight and wind-tunnel results occurred in the longitudinal-stability data. The flight results for both airplanes indicated a 5 percent greater stability margin than the tunnel results. In addition, the transonic stability break for airplane A occurred at a Mach number of 0.85 in flight compared with a Mach number of 0.90 in the wind tunnel.

There were many similarities between the measured values of the stability derivatives for the two airplane configurations. However, in some cases the stability derivatives measured in flight for the two airplane configurations had markedly different transonic trends. For example,

the transonic aerodynamic-center shift was considerably greater for airplane B than for airplane A. The pitch damping of airplane A decreased slowly with increasing Mach number while that of airplane B increased. However, the larger part of the apparent improvement in the pitch damping of airplane B at Mach numbers between 0.95 and 1.23 was caused by control motion produced by the response-feel system when the pilot relaxed his grip on the stick during the pitching oscillation. With yaw dampers turned off, airplane B had less damping in yaw than airplane A, and at transonic speeds, the values of $C_{n_r} - C_{n_{\dot{\beta}}}$ for airplane B fluctuated erratically between small positive and negative values.

Langley Research Center,
National Aeronautics and Space Administration,
Langley Field, Va., October 27, 1958.

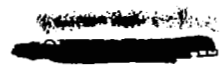

REFERENCES

1. Wolowicz, Chester H.: Dynamic Longitudinal Stability Characteristics of a Swept-Wing Fighter-Type Airplane at Mach Numbers Between 0.36 and 1.45. NACA RM H56H03, 1957.

2. Wolowicz, Chester H.: Time-Vector Determined Lateral Derivatives of a Swept-Wing Fighter-Type Airplane With Three Different Vertical Tails at Mach Numbers Between 0.70 and 1.48. NACA RM H56C20, 1956.

3. Larrabee, E. E.: Application of the Time Vector Method to the Analysis of Flight Test Lateral Oscillation Data. FRM No. 189, Cornell Aero. Lab. Inc., Sept. 9, 1953.

4. Klawans, Bernard B., and White, Jack A.: A Method Utilizing Data on the Spiral, Roll-Subsidence, and Dutch Roll Modes for Determining Lateral Stability Derivatives From Flight Measurements. NACA TN 4066, 1957.

5. Pierpont, P. Kenneth: Transonic Wind-Tunnel Investigation of Static Longitudinal and Lateral Stability and Control Characteristics and Drag Rise of a Representative Fighter Airplane. NASA MEMO 12-14-58L, 1958.

6. Bielat, Ralph P.: A Transonic Wind Tunnel Investigation of the Performance and of the Static Stability and Control Characteristics of a Model of a Fighter-Type Airplane Which Embodies Partial Body Indentation. NASA MEMO 12-13-58L, 1958.

7. Kraft, Christopher C., Jr., McLaughlin, Milton D., White, Jack A., and Champine, Robert A.: Flight Measurements of Some of the Flying Qualities and Stability Derivatives of a Supersonic Fighter Airplane. NASA MEMO 10-7-58L, 1958.

8. Cochi, R. J.: Transonic Wind Tunnel Tests of a 1/21 Scale Model of the Grumman Design 98J Airplane. Rep. No. AA-1140-W-2(Contract No. SC-123 P. O. F87082), vols. I and II, ser. VI, Cornell Aero. Lab., Inc., July 1957.

[redacted]

TABLE I.- PERTINENT DIMENSIONS OF AIRPLANE A

Wing (not including leading-edge chord-extension):	
Area, sq ft	375
Span, ft	35.67
Aspect ratio	3.4
Taper ratio	0.247
Sweepback of quarter-chord line, deg	42
Dihedral, deg	-5.0
Geometric wing incidence, relative to fuselage reference line:	
Cruise and high speed, deg	-1.0
Take-off and landing, deg	7.0
Wing-hinge-point location, percent $\bar{c}$	39.58
Mean aerodynamic chord, in.	141.4
Airfoil section parallel to plane of symmetry:	
Root	NACA 65A006
Tip	NACA 65A005
Deflections of leading-edge droop:	
Inboard section:	
Landing and take-off, deg	25
Cruise, deg	6.75
High speed, deg	0
Outboard section:	
Landing and take-off, deg	27
Cruise, deg	7.0
High speed, deg	0
Chord-extension area (both sides), sq ft	10.33
Center-section inboard flaps:	
Area (both sides), sq ft	13.44
Deflection for landing and take-off, deg	20.0
Deflection for cruise and high-speed, deg	0
Ailerons:	
Chord, percent of wing chord:	
Outboard	28.0
Inboard	23.5
Area, sq ft	20.78
Deflections:	
High speed and cruise, deg	±15
Take-off and landing:	
Both ailerons drooped as flaps, deg	20
As ailerons, deg	+45 to -15
Vertical stabilizer (based on area extending to horizontal-tail center line, not including dorsal):	
Area, sq ft	109
Span, ft	12.75
Aspect ratio	1.5
Sweepback of quarter-chord line, deg	45.0
Taper ratio	0.25
Mean aerodynamic chord, in.	114.8
Tail length, from 25 percent $\bar{c}$ to 25 percent $\bar{c}_t$, in.	173.1
Airfoil section:	
Root	Modified NACA 65A005.3
Tip	Modified NACA 65A004
Rudder:	
Area, sq ft	12.56
Chord, constant, in.	21.28
Maximum deflections:	
High-speed and cruise, deg	±6.0
Take-off and landing, deg	±17.0
Horizontal-tail (based on area extending to fuselage center line):	
Area, sq ft	93.4
Span, ft	18.1
Aspect ratio	3.5
Taper ratio	0.148
Sweepback of quarter-chord line, deg	45
Geometric dihedral, deg	5.417
Mean aerodynamic chord, in.	73.4
Tail length from 25 percent $\bar{c}$ to 25 percent $\bar{c}_t$, in.	204.8
Maximum deflections:	
Trailing edge down, deg	8
Trailing edge up, deg	32
Airfoil section:	
Root	NACA 65A006
Tip	NACA 65A004
Weight and balance:	
Center-of-gravity range (for tests), percent $\bar{c}$	26.5 to 27
Weight:	
Take-off, lb	26,077
Test range, lb	24,500 to 20,000
Range of moment of inertia of airplane about X stability axis, slug-ft^2	11,400 to 10,600
Range of moment of inertia of airplane about Y stability axis, slug-ft^2	89,500 to 82,500
Range of moment of inertia of airplane about Z stability axis, slug-ft^2	97,250 to 90,000
Range of product of inertia referred to X and Z stability axes, slug-ft^2	5,200 to 500

[redacted]

[redacted]

TABLE II.- PERTINENT DIMENSIONS OF AIRPLANE B

Wing:	
Area, sq ft	250
Span, ft	31.625
Aspect ratio	4
Taper ratio	0.5
Sweepback at quarter-chord line, deg	35
Dihedral, deg	-2.5
Incidence, deg	0
Mean aerodynamic chord, in.	98.38
Airfoil section parallel to plane of symmetry:	
Wing root	Modified NACA 65A006
Wing tip	Modified NACA 65A004
Slat area, sq ft	16.8
Slat travel, deg	20
Flap area, sq ft	35.82
Flap travel (down), deg	30
Flaperon area (total), sq ft	21.3
Flaperon travel (up), deg	55
Vertical stabilizer:	
Area (exposed fin), sq ft	45.1
Span, from fuselage reference line, ft	128
Sweepback of quarter-chord line, deg	45.5
Taper ratio	0.286
Airfoil section	Modified NACA 16.005.625
Rudder:	
Area, sq ft	6.1
Travel (clean condition), deg	±5
Horizontal tail:	
Area (exposed), sq ft	65.5
Span, ft	15.167
Aspect ratio	3.5
Taper ratio	0.4
Sweepback of quarter-chord line, deg	35
Dihedral, deg	0
Mean aerodynamic chord, in.	55.13
Tail length from 25 percent $\bar{c}$ to 25 percent $\bar{c}_t$ ($\bar{c}_t$ based on including fuselage area), in.	151.23
Maximum deflections:	
Trailing edge down, deg	5
Trailing edge up, deg	18
Airfoil section:	
Root	NACA 65A006
Tip	NACA 65A004
Weight and balance:	
Center-of-gravity range (for tests), percent $\bar{c}$	24 to 25
Weight:	
Take-off, lb	20,000
Test range, lb	18,000 to 16,000
Range of moment of inertia about the X stability axis, slug-ft^2	6,500 to 6,300
Range of moment of inertia about the Y stability axis, slug-ft^2	44,400 to 41,000
Range of moment of inertia about the Z stability axis, slug-ft^2	49,000 to 43,800
Range of product of inertia referred to the X and Z stability axes, slug-ft^2	-2,900 to -2,500

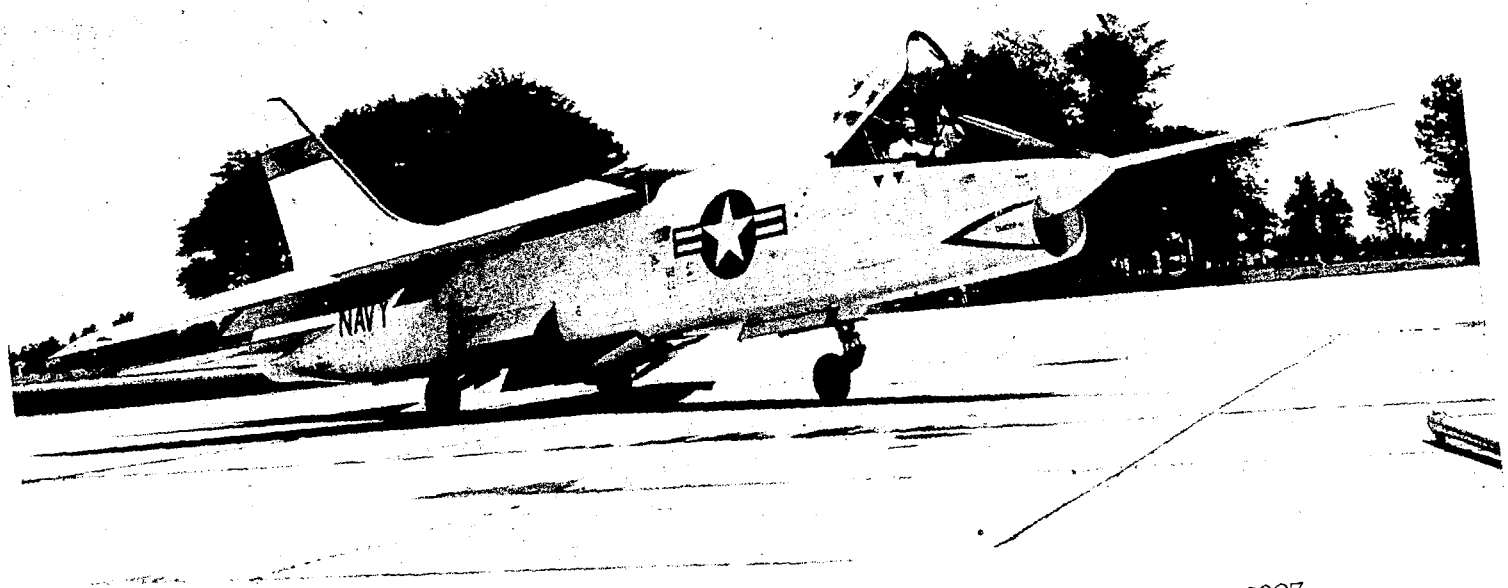

L-57-2097

(a) Three-quarter front view.

Figure 1.- Photographs of airplane A.

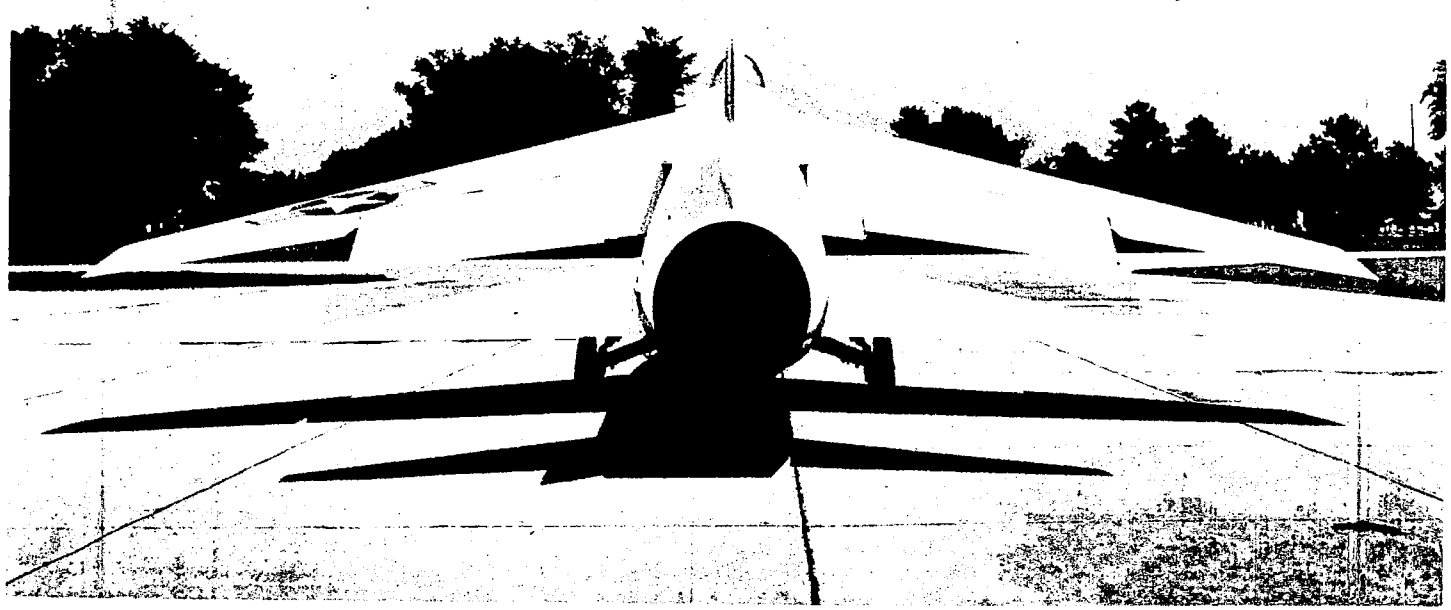

(b) Rear view. L-57-2102

Figure 1.- Concluded.

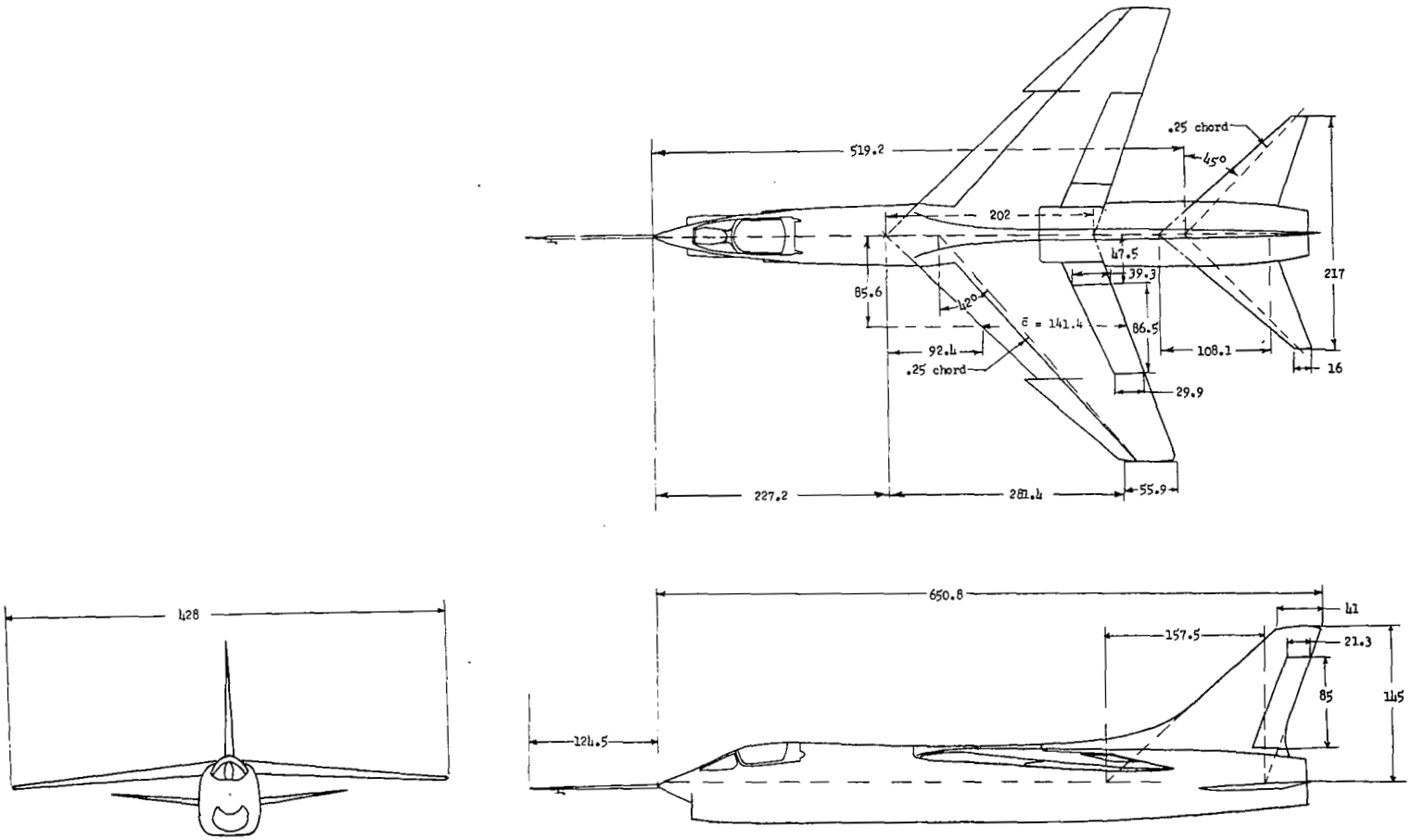

Figure 2.- Three-view drawing of airplane A. All linear dimensions are in inches. (For detailed dimensions, see table I.)

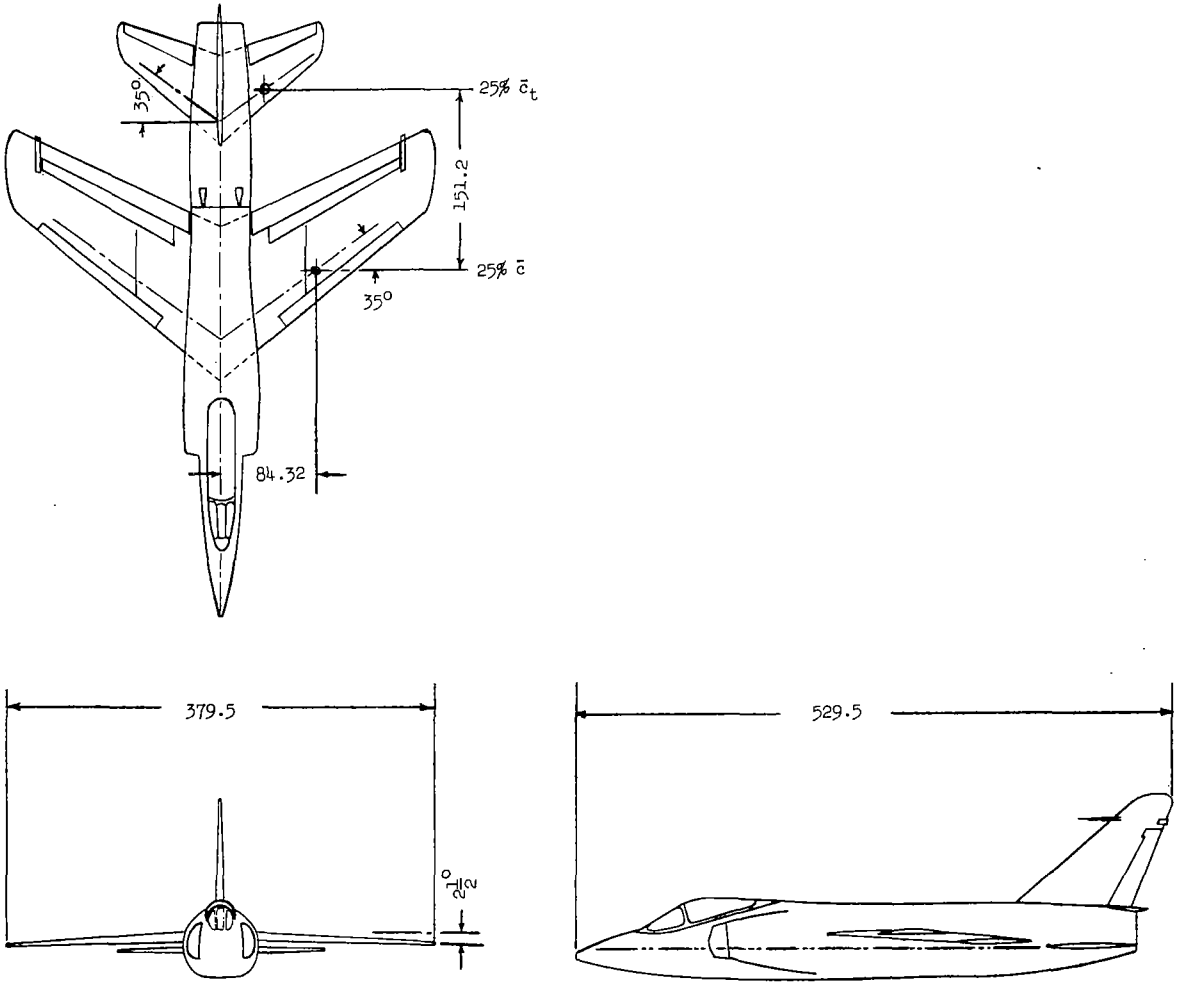

Figure 3.- Three-view drawing of airplane B. All linear dimensions are in inches. (For detailed dimensions, see table II.)

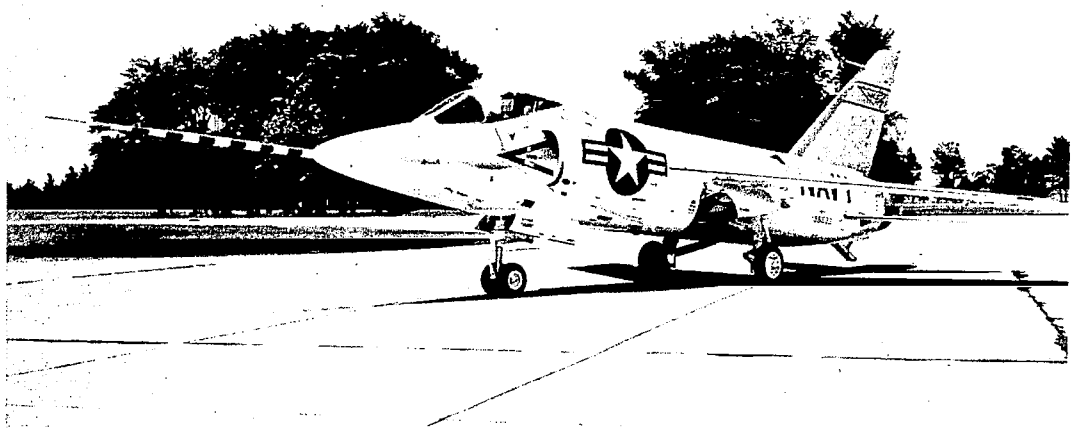

(a) Three-quarter front view. L-57-2254

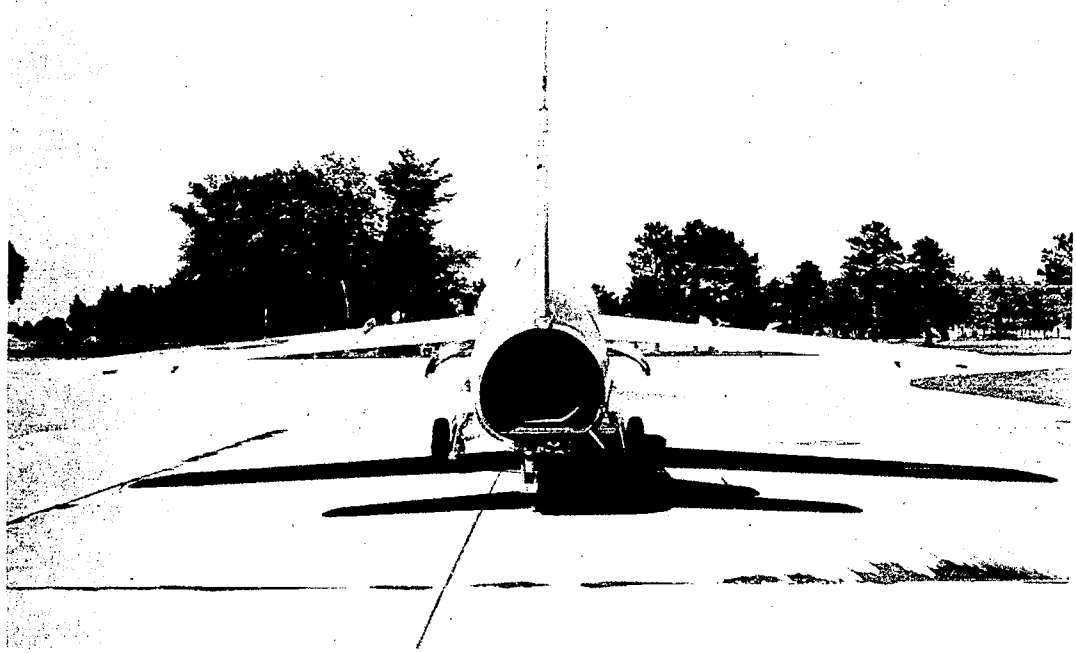

(b) Rear view. L-57-2256

Figure 4.- Photographs of airplane B.

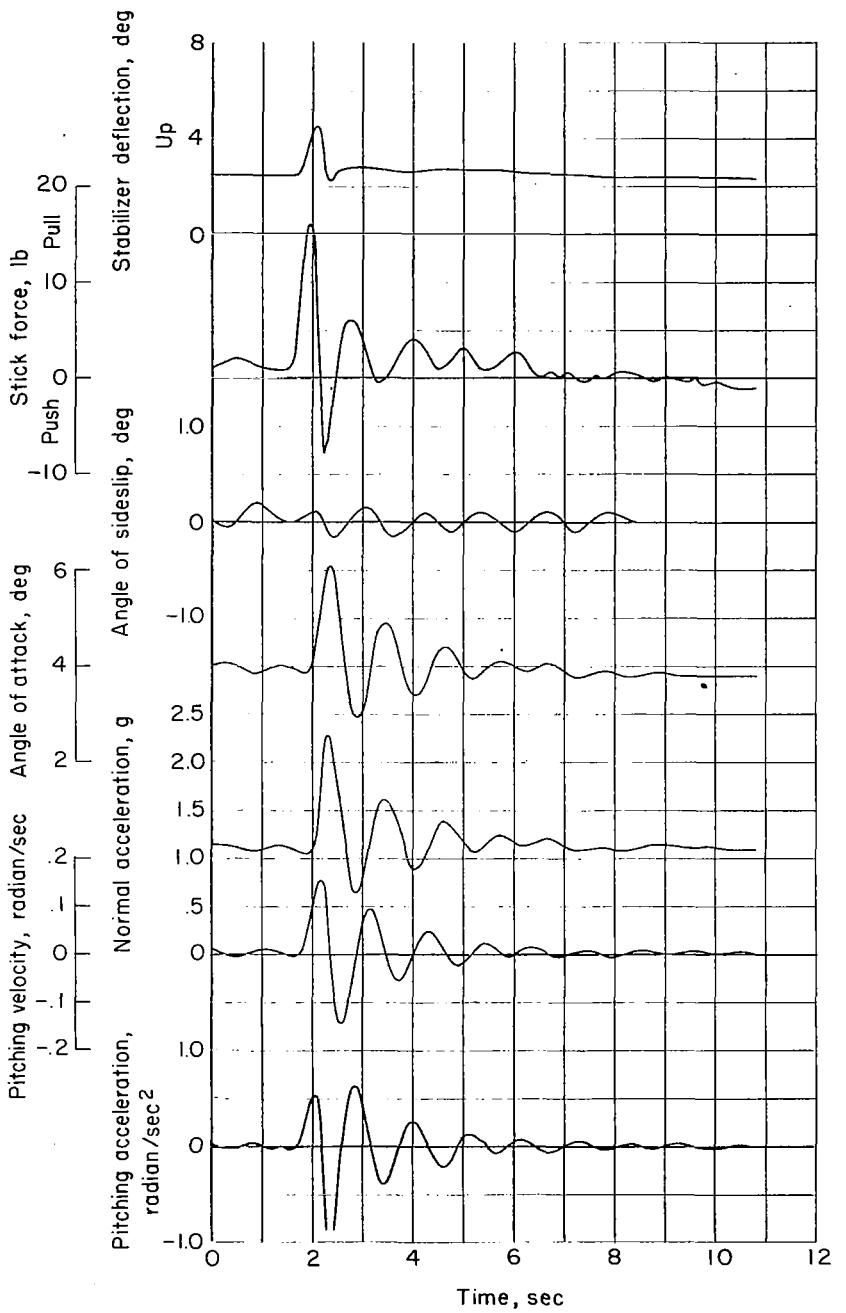

Figure 5.- Time history of a short-period longitudinal oscillation of airplane B at a Mach number of 1.0 and an altitude of 35,000 feet. (Trace amplitudes have been enlarged up to five times from the film records.)

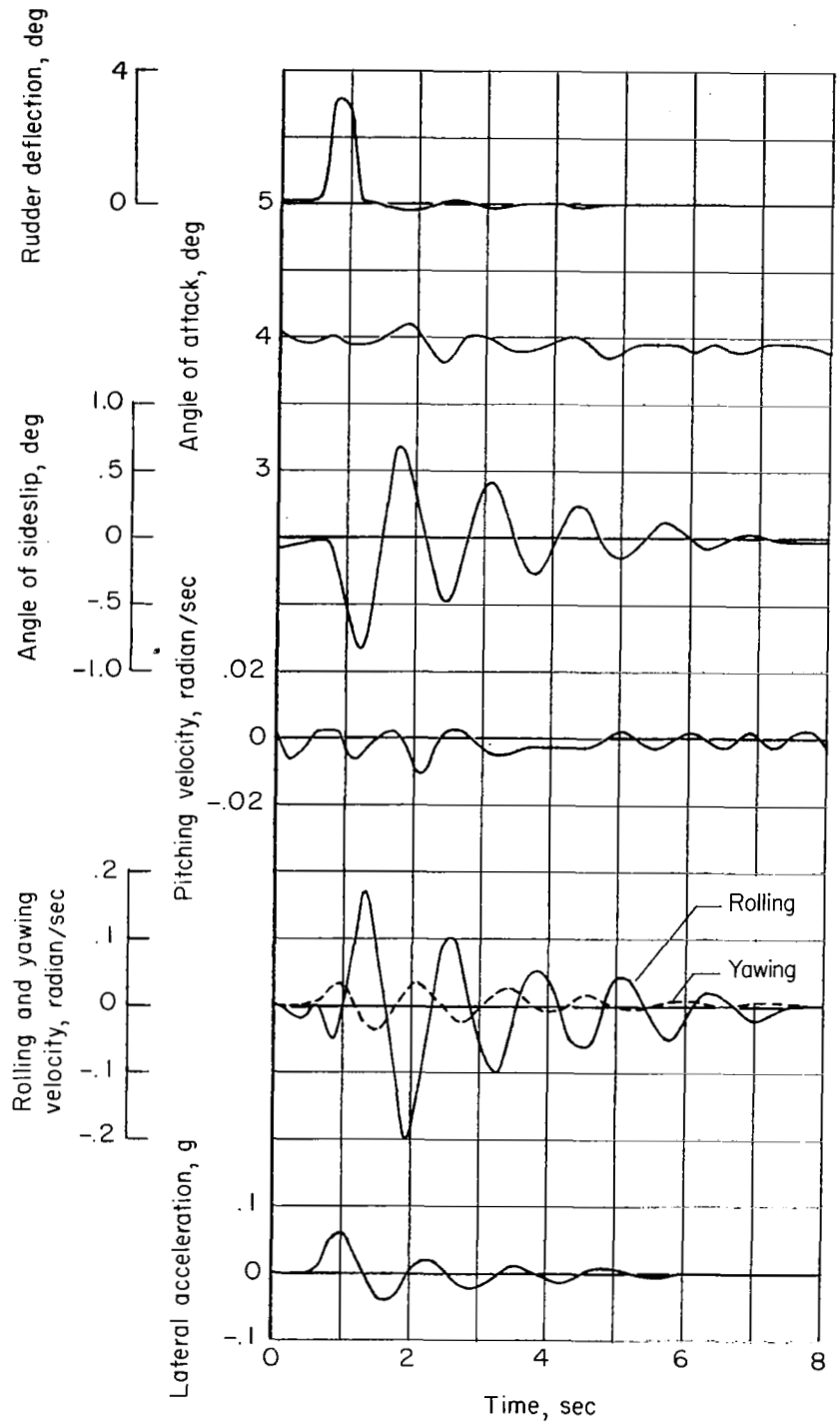

Figure 6.- Time history of a short-period directional oscillation of airplane B at a Mach number of 1.15 and an altitude of 35,000 feet. (Trace amplitudes have been enlarged up to ten times from the film records.)

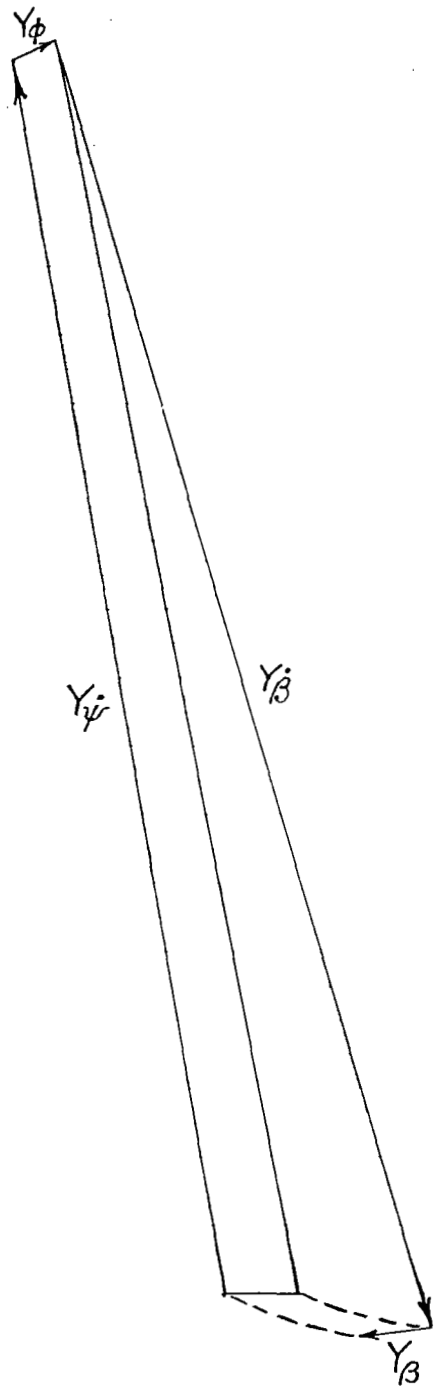

Figure 7.- Sample side-force vector diagram which illustrates the adjustment of the β and $\dot{\beta}$ vectors to satisfy the side-force equation.

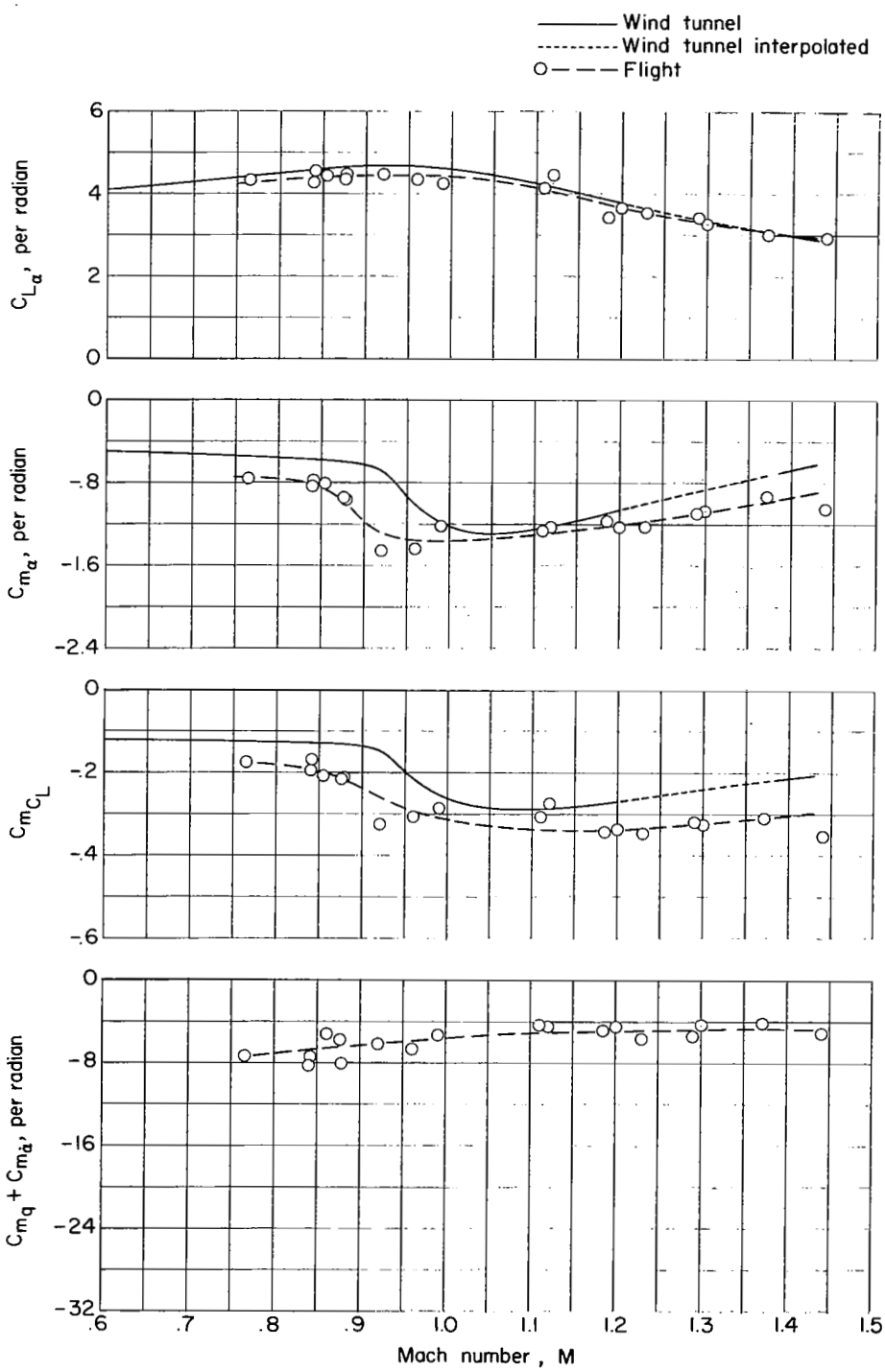

Figure 8.- Longitudinal stability derivatives for airplane A.

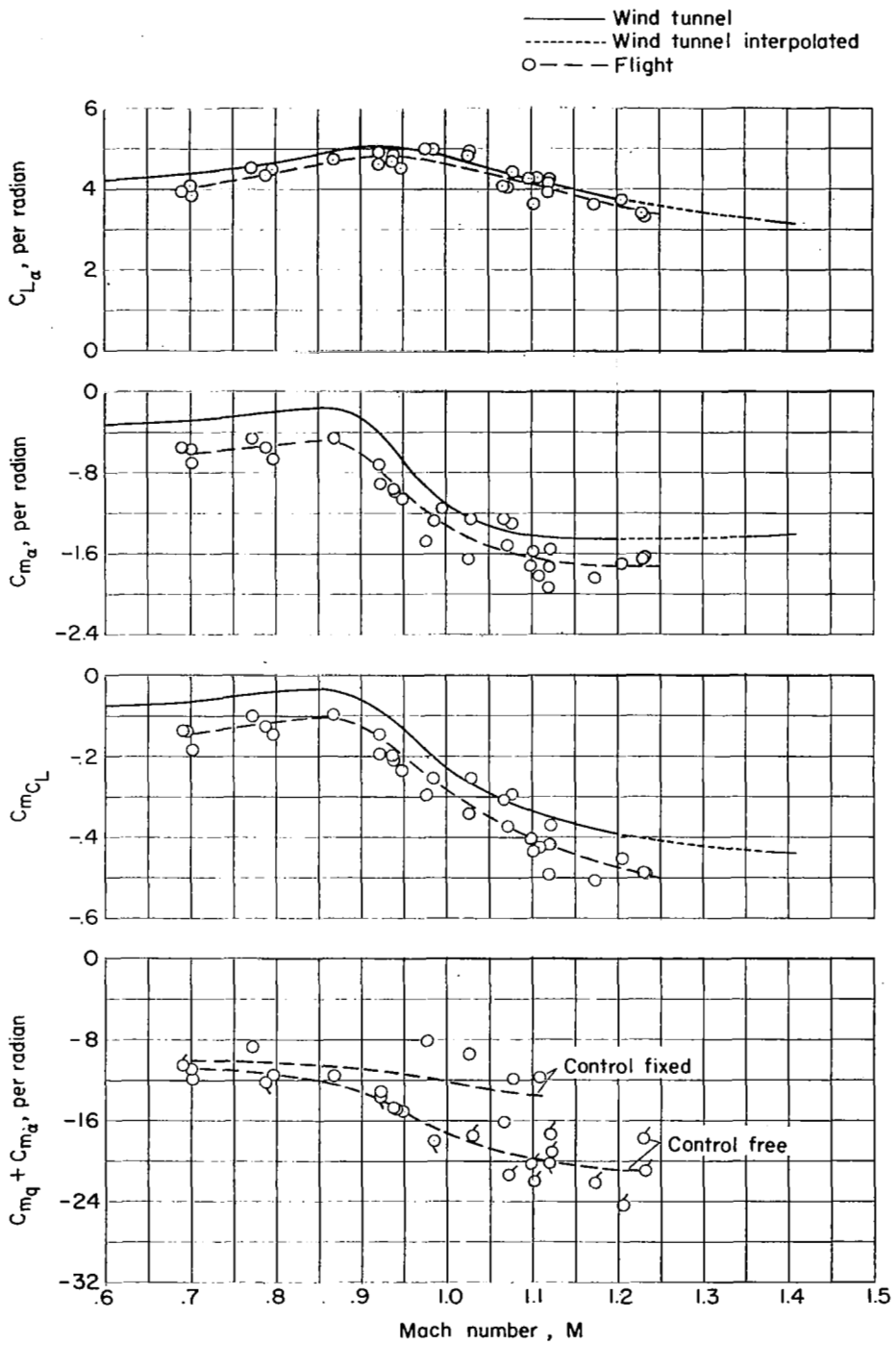

Figure 9.- Longitudinal stability derivatives for airplane B.

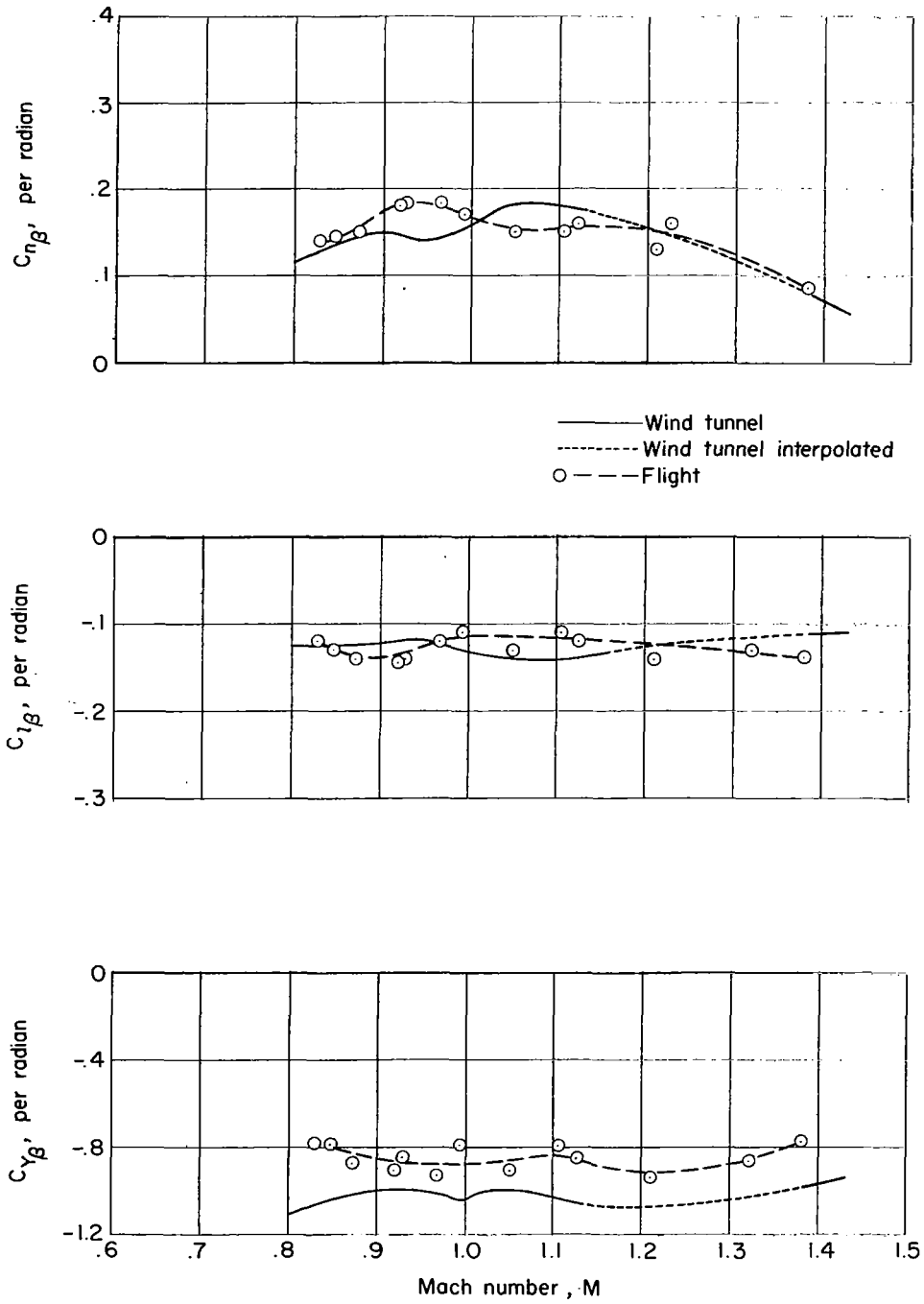

Figure 10.- Static lateral stability derivatives for airplane A.

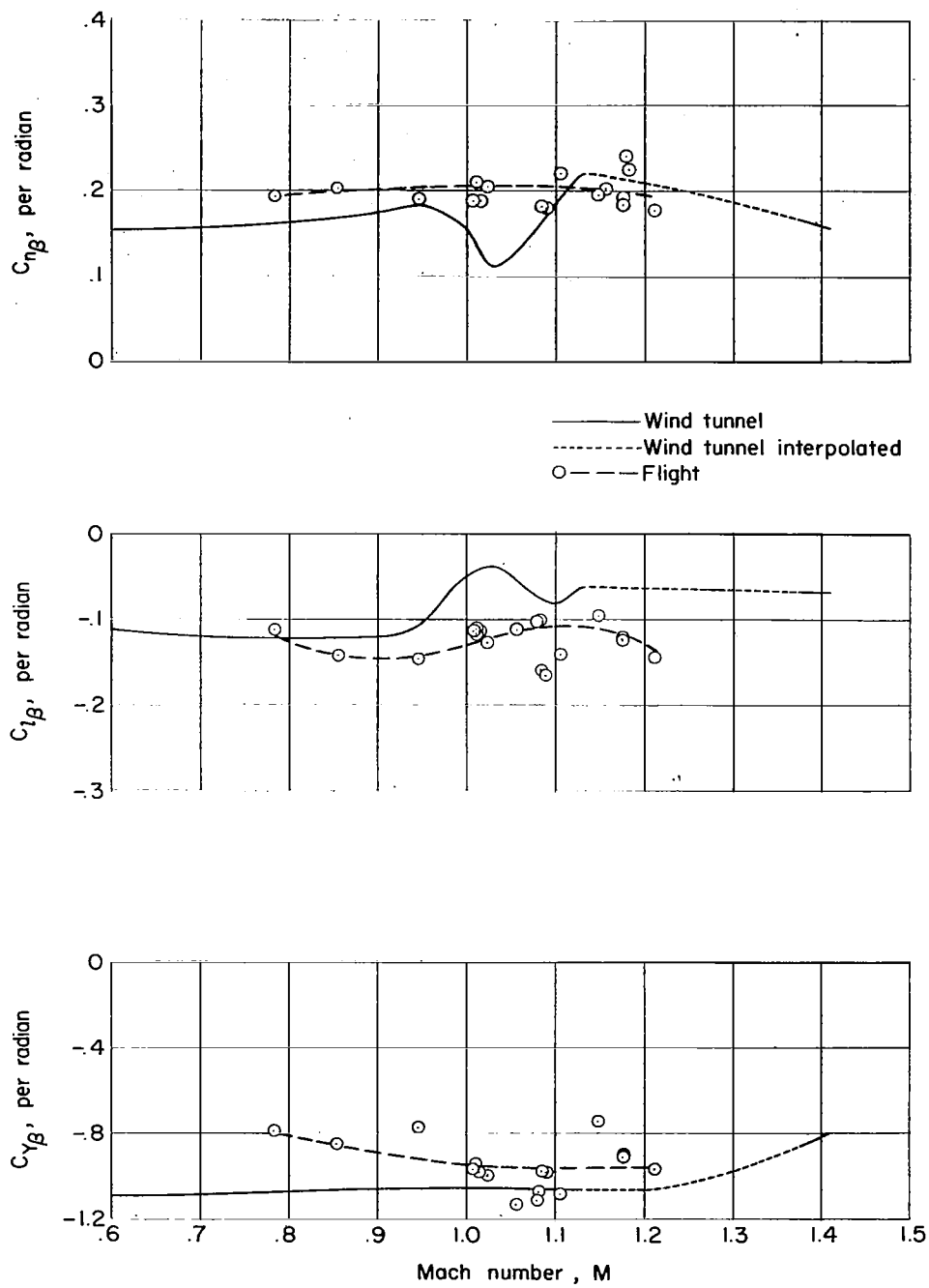

Figure 11.- Static lateral stability derivatives for airplane B.

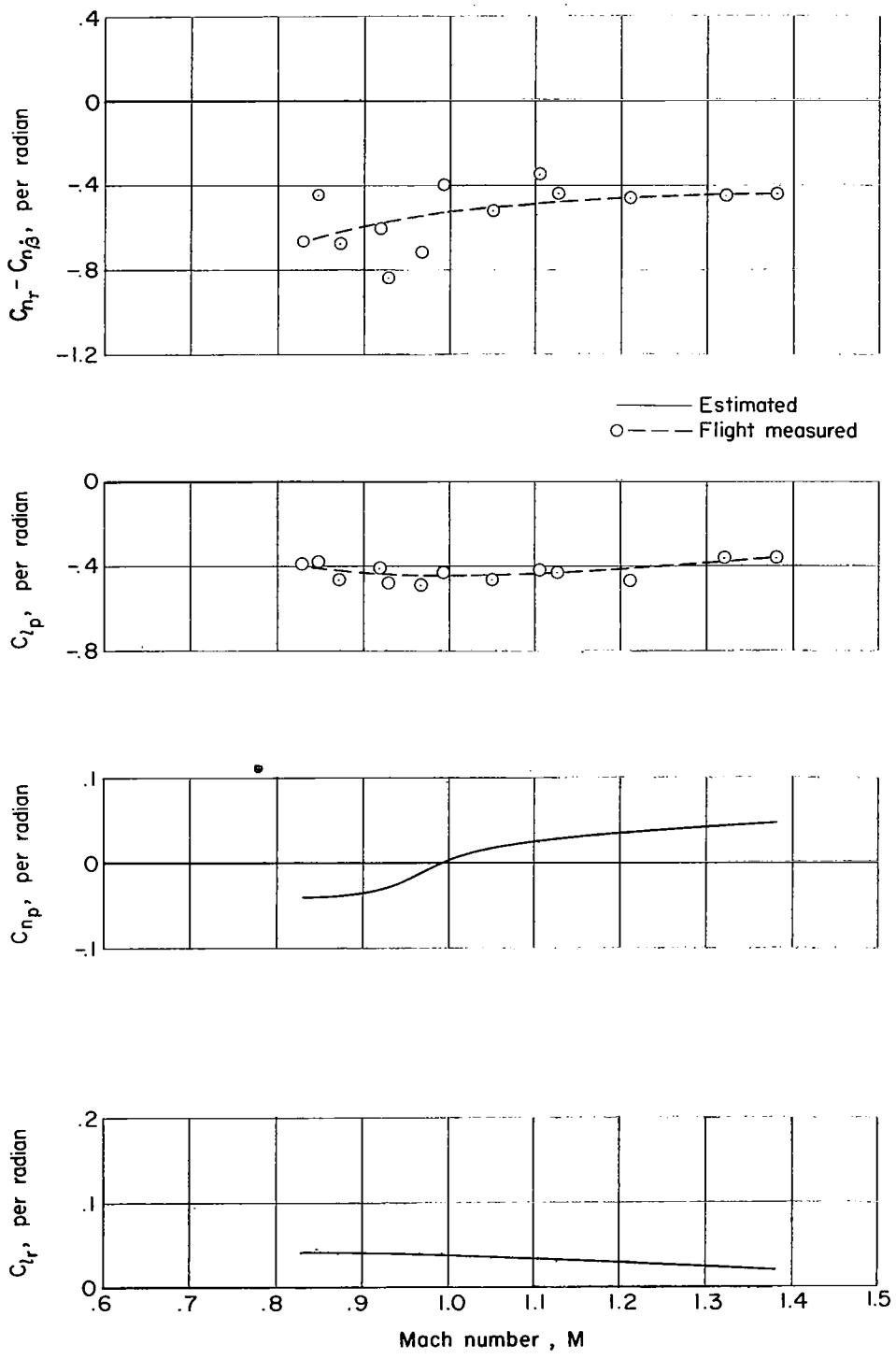

Figure 12.- Rotary and damping derivatives for airplane A.

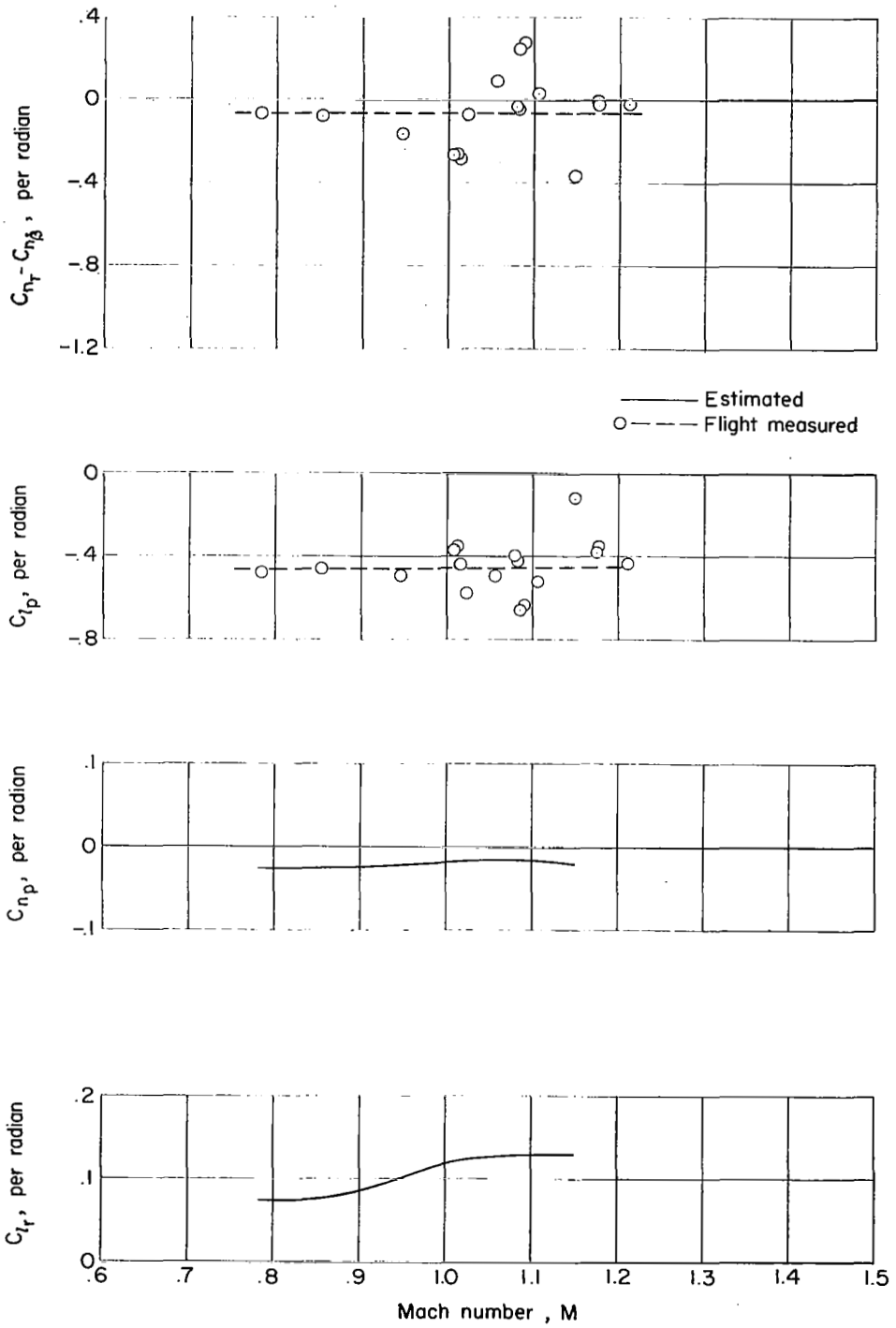

Figure 13.- Rotary and damping derivatives for airplane B.